

RESEARCH PAPER

Optimization of Electrospinning Conditions for Magnetic Poly (acrylonitrile- co- acrylic acid) Nanofibers

Nafiseh Sabzroo¹, Tahereh Rohani Bastami^{1*}, Majid Karimi² and Tahereh Heidari³

¹ Department of Chemical Engineering, Quchan University of Technology, Quchan, Iran

² Department of Polymerization, Faculty of Sciences, Iran Polymer and Petrochemical Institute, Tehran, Iran

³ Department of Chemistry, Faculty of Sciences, Ferdowsi University of Mashhad, Iran

ARTICLE INFO

Article History:

Received 19 September 2018

Accepted 10 January 2019

Published 01 April 2019

Keywords:

Electrospinning

Magnetic Nanoparticle

Nanofibers

Poly (acrylonitrile-co-acrylic acid)

ABSTRACT

Magnetic poly (acrylonitrile-co-acrylic acid) (PAN-co-AA) composite nanofibers with different proportions of magnetic nanoparticles (MNPs) were fabricated using electrospinning technique. Electrospinning conditions like polymeric concentration, applied voltage, feeding rate, working distance, and collector type were explored and optimized to produce ultrafine- uniform size and bead free nanofibers. Electrospun nanofibers were characterized by scanning electron microscopy (SEM), energy dispersive X-ray spectroscopy (EDX), Brunauer–Emmett–Teller (BET) isotherms, X-ray diffraction (XRD), fourier transform infrared spectroscopy (FTIR) and vibrating sample magnetometry (VSM). The optimum electrospinning conditions were obtained to be 12wt% concentration, 20 kV voltages, 20 cm tips to collector distance and 0.5 mL/h flow rate. At the optimal operating condition the nanofibers diameter dropped from 359 nm to 74 nm and the specific surface area increased to 12.09 m²g⁻¹ with respect to MNPs content (0 to 40 wt. %). Also, the magnetic property of magnetic nanofibers facilitated the separation of solid phase much easier than nonmagnetic nanofiber.

How to cite this article

Sabzroo N, Rohani Bastami T, Karimi M, Heidari T. Optimization of Electrospinning Conditions for Magnetic Poly (acrylonitrile- co- acrylic acid) Nanofibers. J Nanostruct, 2019; 9(2): 301-315. DOI: 10.22052/JNS.2019.02.012

INTRODUCTION

Electrospinning is an efficient method for the production of nonwoven nanofibers ranging from 5 to 500 nm in diameter [1]. Due to their large surface area to volume ratio and types of morphology, nanofibers have been extensively used in various areas [2-8].

The morphology and surface properties of electrospun nanofibers are affected by several factors including solution properties (polymer concentration, solvent type, viscosity and conductivity), presence of nanoparticles in polymeric solution, electrospinning conditions (applied voltage, feeding rate and distance

between capillary tip and collector type), and ambient conditions (temperature and relative humidity), many research groups have examined the role of these conditions in nanofiber structures [9].

Recently, PAN-co-AA has been the subject of growing attention in fiber preparation [10] (Table S1, supplementary file). Some specifications of this copolymer such as, ease of production, solubility in inexpensive solvents, insolubility in water, high capacity for pollutants adsorption (caused by carbonyl (C=O) and carboxyl groups (C=O) on their surface), high biocompatibility, and pH sensitivity, have led to many studies about the

* Corresponding Author Email: t.rohani@qiet.ac.ir

PAN-co-AA nanofibers [11-12]. For example, Guo et al. [13] showed that the mean diameter of PAN nanofibers was raised by increasing of PAN concentration solution and applied voltage. Zhi-Kang Xu et al. [14] found that an increase in the polymeric concentration of PAN-co-AA, led to the change in the shape of beads from spherical to spindle-like structures. The results about the effect of nanoparticles on nanofibers structures are heterogeneous. Zhou et al. [15] showed that the size and smoothness of the pure PAN nanofibers changed slightly with a rise in the FeCl_2 content. Also, it was found that the roughness of PAN-co-AA nanofiber can be changed into smoothness in the presence of carbon nanotube [16]. Also, it was found that these effects are caused by the competition between the solution viscosity and the electrical conductivity. However, Kim et al. [10] and Bayat et al. [17] suggested that fiber morphology of PAN did not change in the absence and presence of carbon quantum dots and Fe_3O_4 nanoparticles, respectively. Wei [18] revealed that the addition of Fe_3O_4 nanoparticles increased the thickness of electrospun fibers.

In the present study, the effects of electrospinning conditions such as polymeric concentration, applied voltage, feeding rate, working distance and collector type were investigated on the morphological appearance of magnetic PAN-co-AA (with molecular weight of 131,000 g/mol) for the first time. Ultrafine-uniform size and bead free nanofibers were prepared on the optimum conditions: 12wt% concentration, 20 kV voltages, 20 cm tips to collector distance and 0.5 mL/h flow rate. At the optimal operating conditions for electrospinning, the role of MNPs content on the nanofibers diameter and specific surface area were explored. It was shown for the first time that, when the Fe_3O_4 mass proportion was increased from 0 to 40 wt. %, the fiber diameter dropped from 359 nm to 74 nm and the specific surface area increased from $9.66 \text{ m}^2 \cdot \text{g}^{-1}$ to $12.09 \text{ m}^2 \cdot \text{g}^{-1}$.

MATERIALS AND METHODS

Anhydrous ferric chloride (FeCl_3), anhydrous sodium acetate (CH_3COONa), α, α' -azobisisobutyronitrile (AIBN), diethylene glycol (DEG), dimethylformamide (DMF), dimethyl sulfoxide (DMSO), acrylonitrile (AN) and acrylic acid (AA) were of analytical grade and purchased from Merck Co., Germany. AIBN was purified by

recrystallization of methanol. Other materials were used as received without further treatment. Milli-Q water was used with a minimum resistivity of $18.2 \text{ M}\Omega \cdot \text{cm}^{-1}$.

Synthesis of PAN-co-AA

Poly (AN- AA) copolymers were synthesized by radical copolymerization in DMSO in the presence of AIBN as follows [19]. AN and AA (mass ratio of 4:1) were dissolved in DMSO with a total monomer to DMSO mass ratio of 4:11. The initiator, AIBN was added to the mixed solution with a weight ratio of 1:450 to the total monomers. After exposing the solution to nitrogen for 1h, polymerization was carried out in an airtight device at 60°C for 6 h. After the reaction, the viscous mixture was progressively added to a large quantity of water to precipitate the crude copolymer. Subsequently, it was washed several times with water and finally soaked in methanol to remove the residual monomers and initiators completely. The final copolymer was dried at 60°C in a vacuum oven for 72 h (with 78.63% efficiency). The intrinsic viscosity of 0.5 wt.% copolymer in DMF was determined by Ubbelodde-type viscometer at 30°C [20-21]. The copolymer molecular weight was estimated according the following equation (Eq. (1)) for PAN in DMF at 30°C [20].

$$[\mu] = 20.9 \times 10^{-5} (\text{dl} / \text{g}) M_v^{0.75} \quad (1)$$

Preparation of electrospinning solution

Fe_3O_4 nanoparticles (NPs) were synthesized with solvothermal approach [23-24]. A specific amount of the as-prepared Fe_3O_4 NPs was ultrasonically dispersed into DMF for 60 min. Copolymer was dissolved in DMF at 60°C overnight. Then, Fe_3O_4 -DMF solution was introduced to the polymeric solution to produce a final solution with Fe_3O_4 mass ratios of 0%, 10%, 25% and 40% respectively (Table 1). Then, the magnetic-polymeric solution was also sonicated for 2h at room temperature.

Electrospun nanofibers preparation

The electrospinning setup for nanofiber fabrication consists of a high-voltage power supply. A plate ($5 \times 5 \text{ cm}^2$) and a rotating drum (5-cm height and 5-cm diameter) were used as the collector for fabricating aligned and random ultrafine fibers. The viscous fluid was added with a syringe (10 mL) using a stainless steel

Table 1. Electrospinning solution

Spinning name	Mass of polymer (g)	Mass of DMF for polymer dissolved (g)	Mass of MNPs (g)	Mass of DMF for dispersed MNPs (g)	Total mass of DMF (g)
1wt. %-0%	0.10	10	-	-	10
4wt. %-0%	0.42	10	-	-	10
6wt. %-0%	0.64	10	-	-	10
8wt. %-0%	0.87	10	-	-	10
12wt. %-0%	1.36	10	-	-	10
15wt. %-0%	1.76	10	-	-	10
20wt. %-0%	2.50	10	-	-	10
12wt. %-10%	1.36	5	0.136	5	10
12wt. %-25%	1.36	5	0.34	5	10
12wt. %-40%	1.36	5	0.544	5	10

spinneret (inner diameter of 0.72 mm), which was connected to the positive electrode of a high-voltage power supply. The negative electrode of the high-voltage power supply was attached to the collector. All experiments were performed at room temperature, with an ambient humidity of 23% to 45% (the humidity percentage was recorded by sensor which was installed in the electrospinning device). Finally, the obtained nanofibers were dried overnight in the vacuum oven at 60°C.

Instrumentation

Intrinsic viscosity $[\eta]$ of copolymers was measured in the DMF solution using an Ubbelohde. To investigate the surface morphology and size of electrospun fibers, the fibrous scaffolds were sputter-coated with gold and visualized with a field emission scanning electron microscope (FESEM, XL-300). SEM images were analyzed using Image J software. The average fiber diameter and fiber orientation were calculated for 300 fibers randomly. The elemental analysis was undertaken by an energy-dispersive X-ray spectrometer (EDX, Oxford Instruments) attached to the SEM. The crystalline-phase compositions of samples were identified by an x-ray powder diffractometric (XRD, Bruker, D8 FOCUS) with Cu Ka radiation. The brunauer–emmett–teller (BET) surface area of the sample was analyzed using a Micromeritics ASAP 2020 nitrogen adsorption apparatus. The functional groups in the composited fibers were identified by Fourier transform infrared (FTIR) spectroscopy using a thermo scientific nicolet iN10 spectrometer (thermo fisher scientific, waltham, MA, USA). The magnetic property of the samples was investigated using VSM (Vibrating sample magnetometer, Leckeshore model).

RESULTS AND DISCUSSION

The presence of willow in electrospun mat nanofiber and its low surface area can reduce the effectiveness of fibers [22]. Thus, to achieve fibers with the minimum diameter, maximum surface area and non-woven format, the electrospinning parameters were examined in this article.

For preparation of bead free nanofiber with minimum diameter, we have to examine all parameters classified in the introduction section. The optimum electrospinning variables were selected for adding nanoparticles and also their role in mats structures were investigated.

Effect of copolymer concentration

All polymeric solution (from 1- 20 wt. %) prepared for electrospinning process are shown in Table 1. The polymeric solution with 1 and 20 wt. % were not suitable for fabrication of fibers because very dilute solution (1 wt. %) dripped from the tip of syringe and the concentrated solution (20 wt. %) could not pass through the needle. The SEM micrographs of pure polymer nanofibers with 4, 6, 8, 12 and 15 wt. % concentrations are shown in Fig. 1.

As shown in this Figure, the nanofibers at 4 wt. % exhibited a mixture of beads and fibers along with thin fibers (mean diameter of 111 nm). These images show numerous nano-sized to micro-sized fibers which were woven (20-400 nm) along the electrospun nanofibers axis. An increase in the concentration of polymeric solution (6 and 8 wt. %) led to the enlarged diameter of fibers and reduced the number of willows. By increasing concentration up to 12 wt % PAN-co-AA, smooth, uniform, continuous and bead-free nanofibers with a mean diameter of 390 nm were fabricated

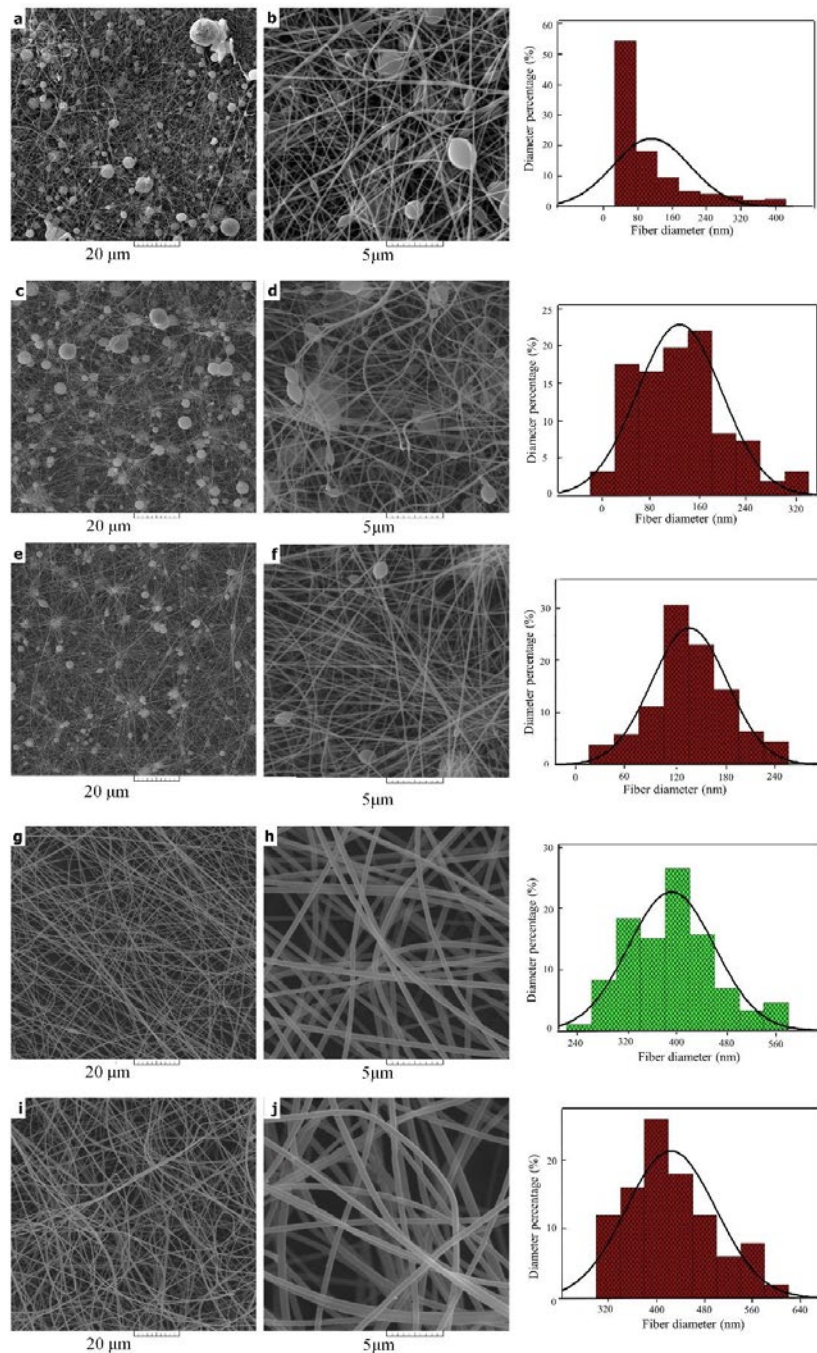


Fig. 1. SEM images and fiber diameter distributions of PAN-co-AA nanofibers at 15kV, distance between nozzle-collector of 200 mm, flow rate of 2 mL/h, with different solution concentrations: (a and b) 4 wt.%, (c and d) 6wt.%, (e and f) 8 wt.%, (g and h) 12 wt.%, and (i and j) 15 wt.%.

(Figs 1g and 1h). The further rise of copolymer concentration to 15 wt. % led to the formation of fibers of greater thickness (424 nm) and regularity (Fig. S1). This confirmed the chain entanglements in the polymeric solution. It was found that for bead-

free and continuous fibers deposit on the collector, a critical viscosity (μ_c) was required [25]. In each dilute solution (1 wt. %) the viscosity was so low that bead was only formed on the collector. When the viscosity of polymeric solution reached critical

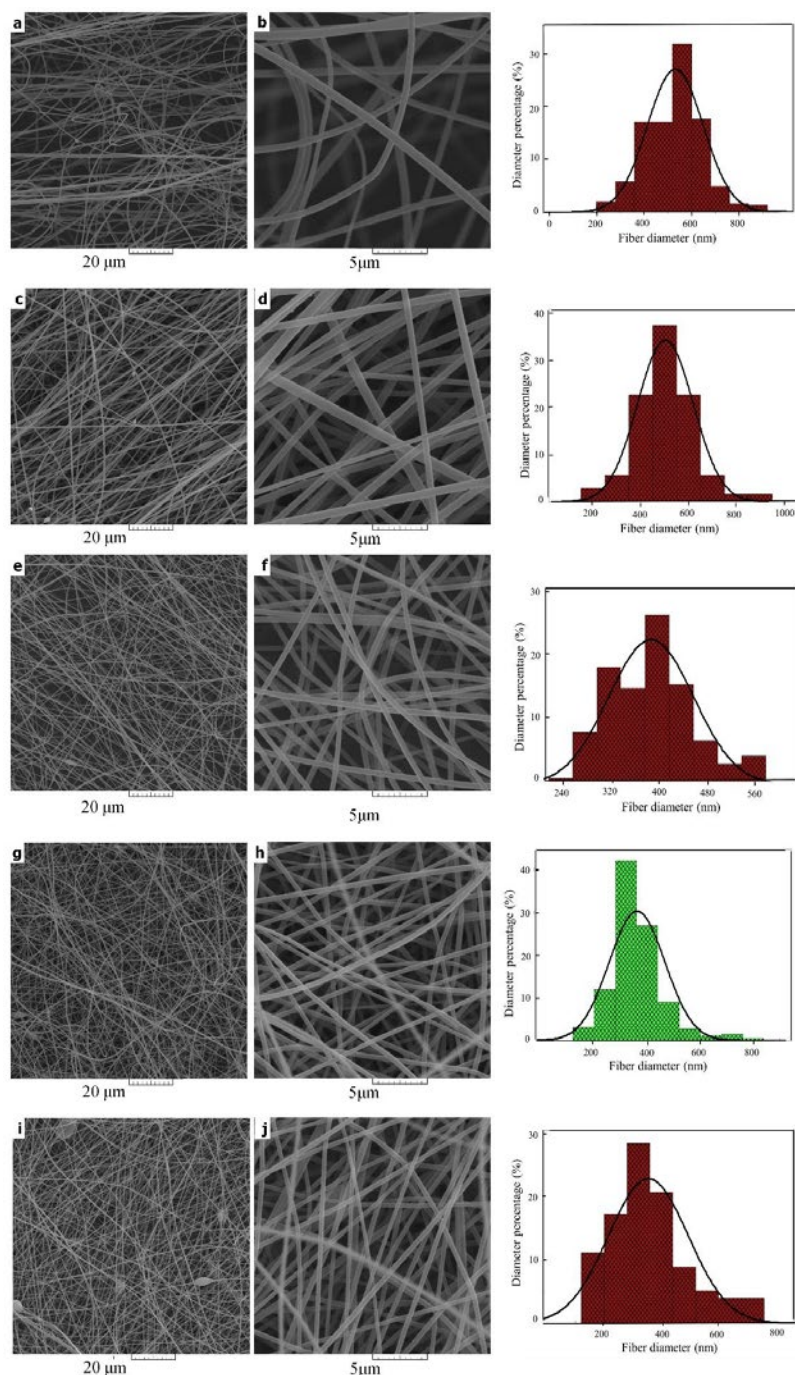


Fig. 2. SEM images and fiber diameter distributions of PAN-co-AA nanofibers at 12wt. %, nozzle-collector of 200 mm, flow rate of 2 mL/h, with different applied voltage: (a and b) 8 kv, (c and d) 10 kv, (e and f) 15 kv, (g and h) 20 kv, and (i and j) 25 kv.

viscosity, the fiber was fabricated and the number of beads declined. As shown in SEM images, by increasing the copolymer concentration, the mean fiber diameter increased (a concentration of 4 wt. % yields fibers of 111 ± 189 nm, 6 wt. % produces fibers of 127 ± 69 nm, and 8 wt.% and

15 wt.% generate fibers of 135 ± 45 , 390 ± 70 and 424 ± 74 nm, respectively.

Since non-woven and relatively regular fibers were achieved in concentrations of 12%, this level of concentration was selected for further study.

Effect of applied voltage

Applied voltage is a crucial parameter in fabrication of electrospun fibers. For stable “Taylor cone” at the needle end and formation of smooth, uniform and continuous nanofiber, this parameter must be optimum. The researchers disagree regarding the effect of voltage on fiber structure. For instance, Zhang et al. reported that PAN fiber diameter increased from 153 to 300 nm with raising applied voltage from 10 to 20 kV [20]. Lanceros et al. [26] showed that PLLA (Poly (L-lactide acid)) diameter dropped when the voltage was raised from 12 to 20 kV and increased at higher voltages (>20kV). As the applied voltage and its effect on fiber structure are a function of the type of polymer, the effect of voltage on formation of electrospun nanofiber was studied. For this purpose, the applied voltage was changed from 8 to 25 kV. The SEM images and fiber diameter distributions of the nanofibers are shown in Fig. 2.

Generally, the electrical field strength is reinforced proportional to the increased applied voltage, which leads to the augmented electrostatic repulsive force on the fluid jet, while the surface tension remains constant. Furthermore, at high voltage, the solution is quickly evaporated from the needle tip and the flight time is reduced. Thus, the polymeric jet do not have sufficient time to align themselves, and therefore broader distribution in terms of nanofiber diameter and bead formation in the fiber are required. In our case, a narrow distribution of nanofiber diameters was obtained at lower voltages (8 to 20 kV), due to higher flight time of the fiber to collector plate. The mean fiber diameter dropped from 536, 503, 390 and 361 nm to 354 nm when the applied voltage was increased from 8, 10, 15, 20 to 25 kV, respectively (Figs. 2, and S2). As can be seen in these figures, nanofibers have smooth morphology with no beads at low voltage (< 20kV), but at high voltage, some beads were formed into the fiber. To produce nonwoven fibers at 20 kV, this applied voltage was selected for further experiments.

Effect of flow rate

SEM micrographs of nanofibers prepared by varying feed rate from 0.5 to 2.5 mL/h are shown in Fig. 3. In the flow rate of 0.5 mL/h, thinner nanofibers with broad distribution (about 50-700 nm) were observed. However, narrow distribution diameters (about 550-750 nm) and

thicker nanofibers were found at higher flow rate (2.5 mL/h). In fact, the volume charge density is a variable of feeding rate, especially at higher polymeric jets, so that with intensified instability, a narrow diameter distribution was observed (Fig. S3). In higher feeding rates, the solvent has no time for evaporation and fibers are been stretched completely. As a result, a thicker fiber is obtained, and fibers are combined to form bead structures. On the contrary, at low feeding rates, due to instability of polymeric jet, bead is observed in fiber morphology. These results have been reported in other studies as well [26-27]. In our case, the mean fiber diameter increased from 225, 336, 359, 361 nm, to 399 nm when feed rate was raised from 0.5, 1, 1.5, 2 mL/h, to 2.5 mL/h, respectively (Figs. 3 and S3). Due to production of nonwoven fibers at the feed rate of 1.5 mL/h, this level of feeding rate was selected for further experiments.

Effect of distance between spinner and collector

It was found that the spinning process was also closely related to the evaporation rate of the solvent [28]. Varying nozzle-collector distances can influence fiber morphology by changing the flight time of liquid jet [25]. Fig. 4 shows fibers fabricated with a working distance at the range of 80 to 250 mm. When spinner and collector are distanced at a range of 80 and 100 mm, thicker and flatter fibers with some beads are produced. Also, a broader distribution fiber diameters was observed. On the other hand, by increasing the distance from 100 mm to 250 mm, cylindrical, straight and uniform nanofibers were fabricated (Fig. S4). Generally, at lower distances, the solvent is not evaporated completely and jet instability increases due to the higher supply of electric voltage. Therefore, by increasing the distance between spinner and collector, uniform and thinner fiber can be fabricated [29]. However, due to the relative decline of applied voltage at very high distance between tip and collector, some beads appeared in the nanofiber structure (Fig. 4). The thinner fibers were formed at long distances, but there was an optimum distance to obtain suitable fibers. The mean fiber diameters were 450, 427, 413, 359 and 301 nm, when the nozzle-collector distances were 80, 100, 150, 200 and 250 mm, respectively (Figs 4 and S4). For the production of bead free and cylindrical nanofiber, 200 mm was selected for further experiments.

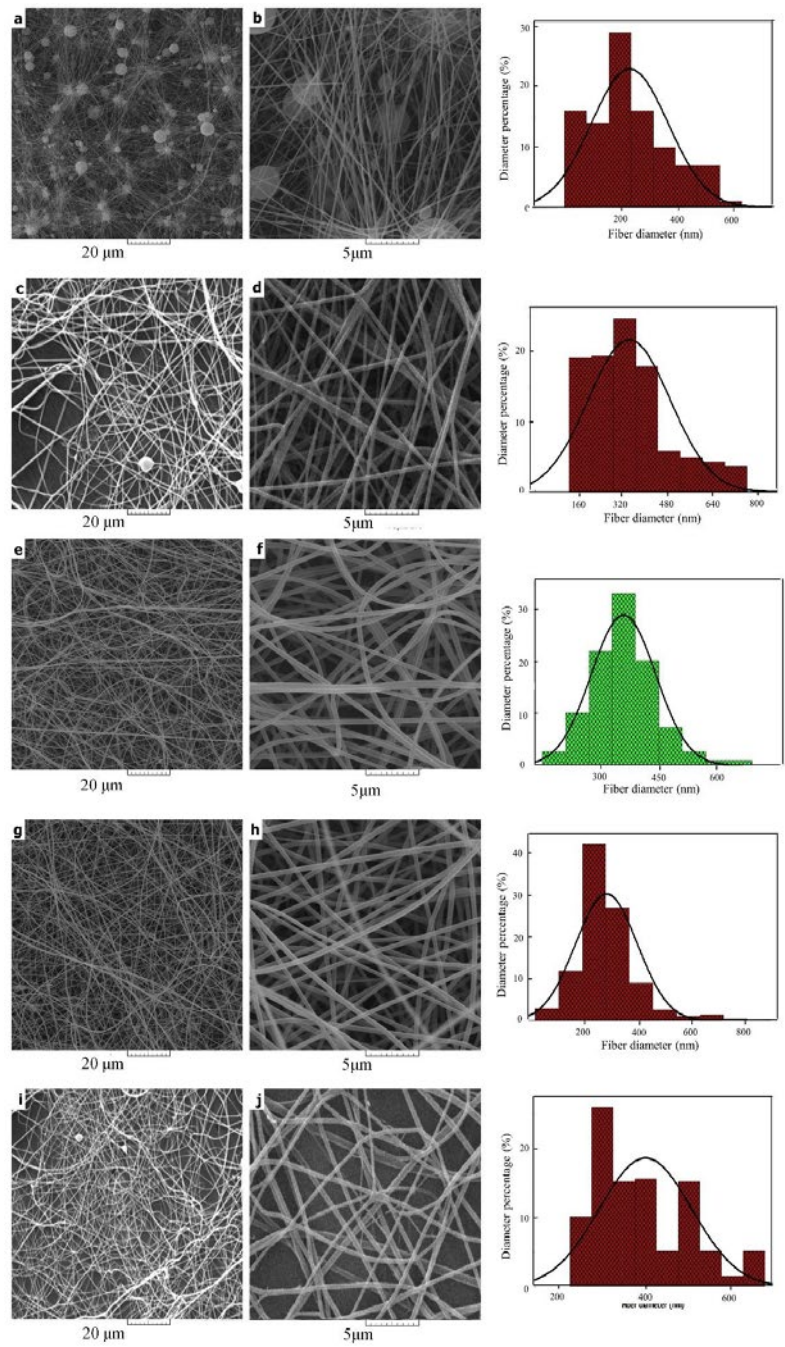


Fig. 3. SEM images and fiber diameter distributions of PAN-co-AA nanofibers at 12wt. %, applied voltage of 20kV, nozzle-collector of 200 mm, with different applied voltage: (a and b) 0.5 mL/h, (c and d) 1 mL/h, (e and f) 1.5 mL/h, (g and h) 2 mL/h, and (i and j) 2.5 mL/h

Effect of collector type and rotation speed

There are different collectors used for fabrication of nanofibers such as plane plate, drum rotatory, grid type, edge type and wire screen [23]. Schima. [30] introduced auxiliary electrodes behind the target to control the width

of deposited and aligned fibers. In addition, it was shown that fibers could be aligned in the gap between two collecting electrodes. Han et al. [21] studied the effect of collector type on fiber morphology, finding that collector type affected on the fiber angle without any significant effect on

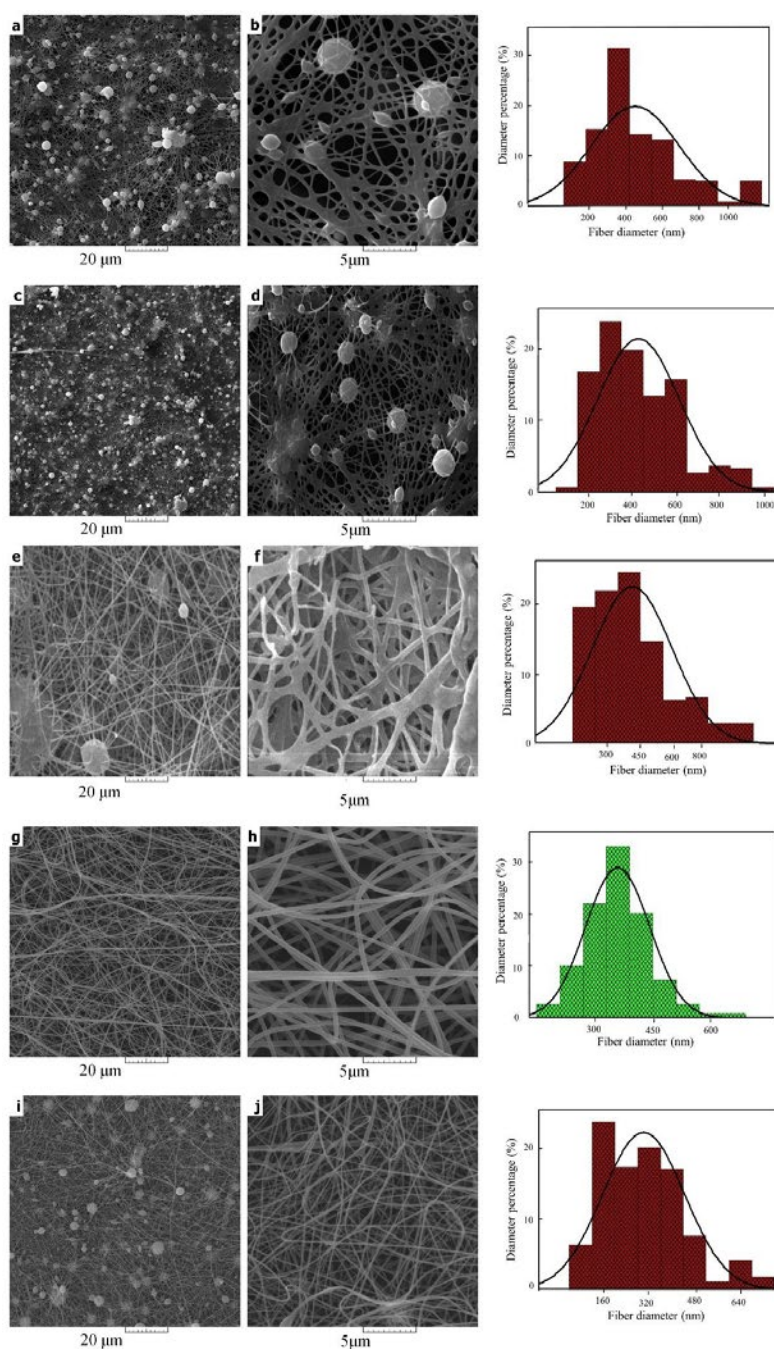


Fig. 4. SEM images and fiber diameter distributions of PAN-co-AA nanofibers at 12wt. %, applied voltage of 20kv, feeding rate of 1.5 mL/h, applied voltage at 20 kv, with different working distance: (a and b) 80 mm, (c and d) 100 mm, (e and f) 150 mm, (g and h) 200 mm, and (i and j) 250 mm.

fiber diameter. Fig. 5. shows morphology, diameter and angle distribution of nanostructured mats, which were obtained using the plate (5×5 cm) and rotating drum (5-cm height, 5-cm diameter) at different rotating speeds. As expected that plane plate collector produced randomly oriented fiber

with some mini jets and fibers on drum rotary collectors were oriented along the same axis. It was expected that fibers with smaller diameter emerge on the drum collector due to greater solvent evaporation, but instead fibers with larger diameter were fabricated. It was suggested

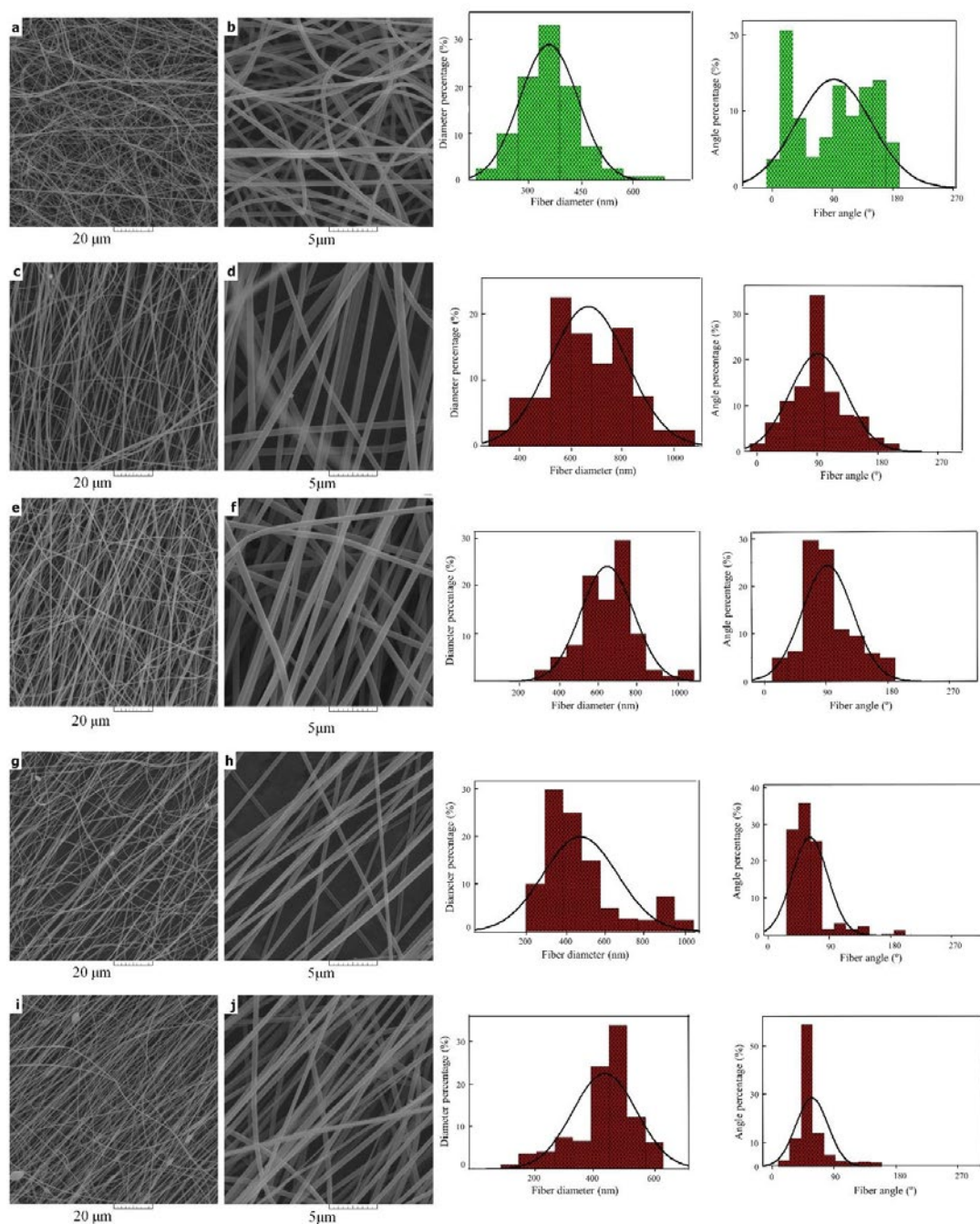


Fig. 5. SEM images and fiber diameter distributions of PAN-co-AA nanofibers at 12wt. %, applied voltage of 20kV, feeding rate of 1.5 mL/h, applied voltage at 20 kV, working distance of 200 mm with different collector type and rotating speed: (a and b) plate 0 rpm, drum (c and d) 500 rpm, (e and f) 1000 rpm, (g and h) 1500 rpm, and (i and j) 2000 rpm.

that divide applied voltage into bigger surface in comparison to the plane plate collector led to the production of fibers with larger diameters. This is consistent with the results reported by previous researchers [31]. Furthermore, in extremely low rotating speed of the collector, the fibers

alignment cannot be initialized, and fibers cause fractures at an extreme rotating velocity [32]. The mean fiber diameter dropped from 359, 666, 643, and 433 nm to 435 nm, respectively, when the rotational speed was raised from 0 (plate collector), 500, 1000, 1500 rpm to 2000 rpm

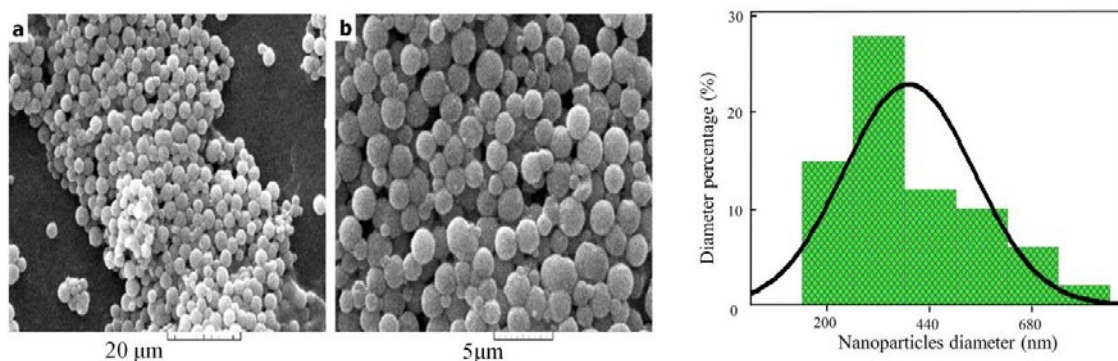


Fig. 6. SEM image and average diameter of magnetic nanoparticles.

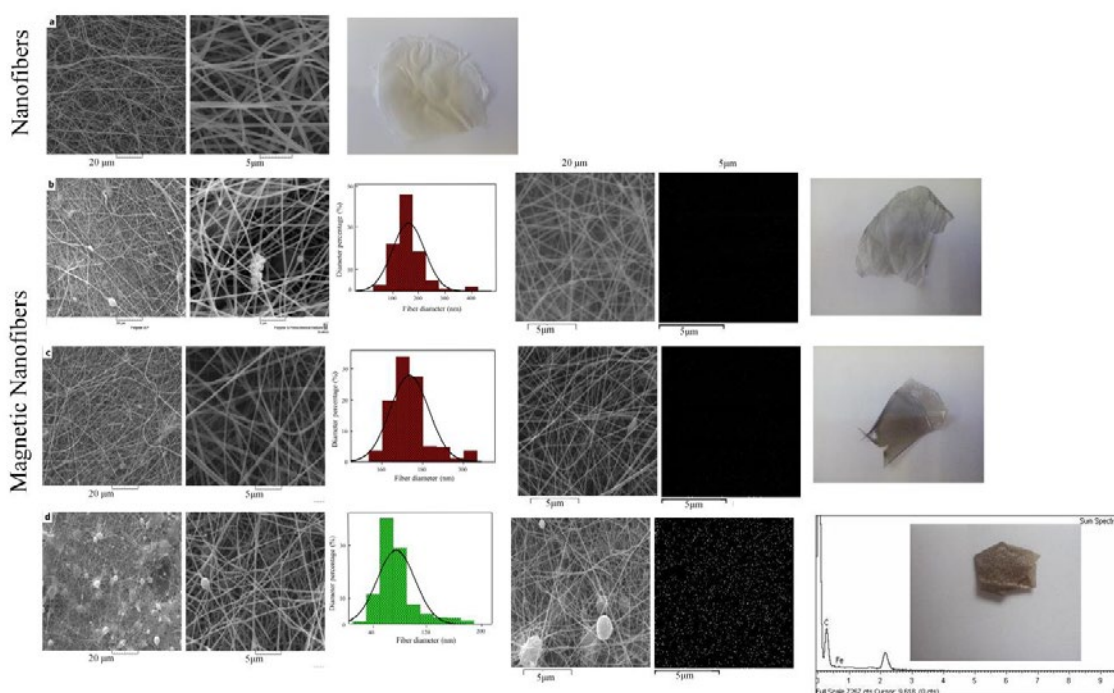


Fig. 7. SEM images, fiber diameter distributions and snapshot of PAN-co-AA/ Fe₃O₄ magnetic nanofibers at 12wt. %, applied voltage of 20kv, feeding rate of 1.5 mL/h, applied voltage at 20 kv, working distance 200 mm at plate, with different mass ratio of MNPs: (a) 10 wt. %, (b) 25 wt. %, and (c) 40 wt. %.

(drum collector) (Figs.5 and S5). With an increase in the rotational speed, the electrical force exerted on the solution rose significantly, while the surface tension remained constant. Hence, lower fiber diameter was obtained when the rotational speed was increased. Also, at high rotating rate of the rotating drum, the smallest fiber was produced, but due to low density, the plate was selected for further study.

Under optimum electrospinning conditions (polymeric concentration of 12 wt. %, applied

voltage of 20kV, feed rate of 1.5 mL/h, tip to collector of 200 mm and plan plate for collector type), nonwoven nanofibers with a fiber diameter of 360 nm and a surface area of 9.66 m².g⁻¹ were produced.

Magnetic nanoparticles effect

The morphology of magnetite particles is shown in Fig. 6. According to the results of SEM, uniform and monodispersed spherical magnetic nanoparticles with a mean diameter of about 390

nm were obtained.

According to Figs. 7 and S6, by increasing magnetic nanoparticles in the polymeric matrix, the fiber diameter was significantly reduced. The mean fiber diameter dropped from 359 nm to 165, 139 and 74 nm, respectively, when the magnetic nanoparticles were increased from 0 to 10, 25, and 40 wt. % (mass ratio of Fe_3O_4 to polymer). It is assumed that diameter reduction is related to the change of properties of polymeric solution such as viscosity, surface tension and conductivity. Also, as shown in Figs. 7 and S6, a narrow diameter distribution was observed with an increase of MNPs in the fiber matrix. EDX images (Fig. 7) confirm the existence of magnetic nanoparticles. Furthermore, as shown in optical images (Fig. 7), the color of mats changed from white to black when the content of Fe_3O_4 nanoparticles in composites increased from 0 to 40 wt.%. This result attributed that, incorporation of MNPs greatly improved mechanical properties of the nanofibers like tensile strength, yield strength, elastic modulus and elongation [33]. In fact, the amount of MNPs has a significant role in the enhancement of mechanical properties, in other words, addition of optimum value of MNPs, (this value is dependent to the type of polymer matrix and the nanoparticle) can increase the tensile strength and Young's modulus, and then , further increase in the MNPs concentration lead to decrease in mechanical properties.

The surface area of magnetic nanofibers (MNFs) (at 40 wt. %) and nanofibers (NFs) were measured by BET surface area analysis and they were obtained 12.09 and $9.66 \text{ m}^2 \text{ g}^{-1}$, respectively (Fig. S7). According to Wang et al. [34], the reduction in nanofiber diameters resulted in increase in the nanofiber surface area by a magnification of nanofiber diameters ratio ($S_2/S_1= r_1/r_2$) S and r are surface area and diameter, respectively). But, it seems that there is not an exact inverse equation between surface area and diameter of nanofibers if the specific surface area of nanofibers calculate from nitrogen absorption/desorption isotherms, BET Isotherms. Eichhorn et al [35], showed that the specific surface area of a fiber network to be overwhelmingly influence by the fraction of the total fiber surface which is in contact with other fibers. They showed that the specific surface area of a network, S_n , is: $S_n = S_f (1 - \Phi)$

In this relation S_f is the specific surface area of a fiber (m^2/g) and Φ determine the fractional contact area of a network. Accordingly, the specific surface area of nanofibers network, which is used in BET test, is lower than the specific area of a nanofiber.

XRD analysis

The crystal structures of Fe_3O_4 nanoparticles, copolymer powder and MNFs (0, 10 and 40 w % of MNPs) were collected (Fig. 8). Based on the XRD

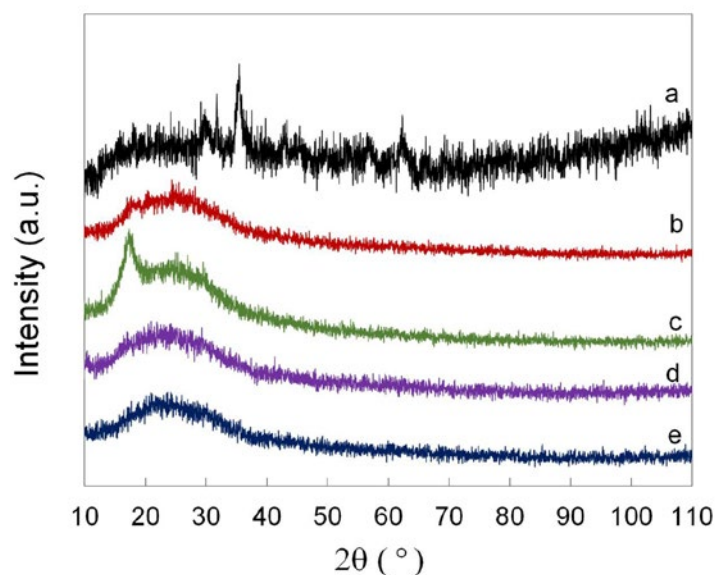


Fig. 8. XRD patterns of the as received (a) magnetic nanoparticles, (b) PANcoAA powder, (c) pure PANcoAA nanofibers, (d) magnetic nanofibers (10 wt. %) and (e) 40 wt. %.

pattern of MNPs (Fig. 8a), the XRD peaks can be indexed to (111), (220), (311), (400), (422), (511), (440), (533), and (642) at 2θ values of 18.2°, 29.5°, 35.5°, 43.3°, 46.8°, 57.1°, 62.3°, 74.4°, and 85.5° for the face center cubic magnetite (Fe_3O_4) structure in accordance with ICDD card of Fe_3O_4 (ICDD-01-089-0951, space group Fd-3m, $a=b=c= 8.49 \text{ \AA}$) [33]. In the case of PAN-co-AA powder (Fig. 8b), the peaks at 2θ value of 17° and 29° corresponded to (100) and (110) plane of PAN and 16.5° for the plane of poly acrylic acid [25]. These results suggest that copolymer was fabricated properly. In the case of electrospun PAN-co-AA nanofibers (Fig. 8c), (100) and (110) phase of PAN shown at $2\theta = 17^\circ$ and 29° , but the XRD peak corresponded to PAA shifted to $2\theta = 21^\circ$ [36-37]. Also, the increased intensity of peaks after spinning process indicated that the electrospinning process enhanced the degree of crystallinity. The enhancement in crystallinity was due to the stretching effect of the applied voltage [36]. From the XRD pattern of magnetic nanofiber with 10 wt. % of MNPs (Fig. 8d), it was observed that peaks at $2\theta = 17^\circ$ (100) and 29° (110) corresponded to PAN segment, and $2\theta = 16^\circ$ corresponded to PAA segment. Also, XRD peaks corresponded to the existence of MNPs on MNFs surface were indicated at $2\theta = 17.05^\circ$ (111), 29.45° (220), 34.1° (311). However, as can be seen

from the spectrum of MNFs with 40 wt. % of MNPs (Fig. 8e), the main characteristic peaks of PAN and PAA are at $2\theta = 17^\circ$ and 30° and $2\theta = 21.7^\circ$, respectively. Moreover, the characteristic peaks of MNPs can be observed in the XRD pattern of MNFs at $2\theta = 17^\circ$ (111), 30.1° (220), 35° (311). Thus, Figs. 8d and 8e confirm the existence of MNPs in the magnetic PAN-co-PAA electrospun nanofibers.

FTIR analysis

FT-IR spectra of the PAN-co-AA powder, Fe_3O_4 nanoparticles and magnetic nanofibers (40 wt. %) are depicted in Fig. S8, and the corresponding functional groups and their absorption wave numbers are listed in Table S2. In Fe_3O_4 nanoparticles spectra (Fig. S8a), the characteristic absorption bands of O-H are shown by the stretching frequency bands at 3419 cm^{-1} , which is consistent with functionalization of nanoparticles [36]. Magnetite nanoparticles were synthesized in the DEG media. The DEG molecules interacted with Fe_3O_4 surface via its C-O-C groups and the corresponding peak appears at 1087 cm^{-1} [38]. Distinct peaks appeared at 586 and 447 cm^{-1} can be assigned to the stretching vibration of Fe-O-Fe and M-O bands [39]. In the case of PAN-co-AA copolymer (Fig. S8b), the peaks at 2242 cm^{-1} and 1718 cm^{-1} indicate the characteristic bands of C=N

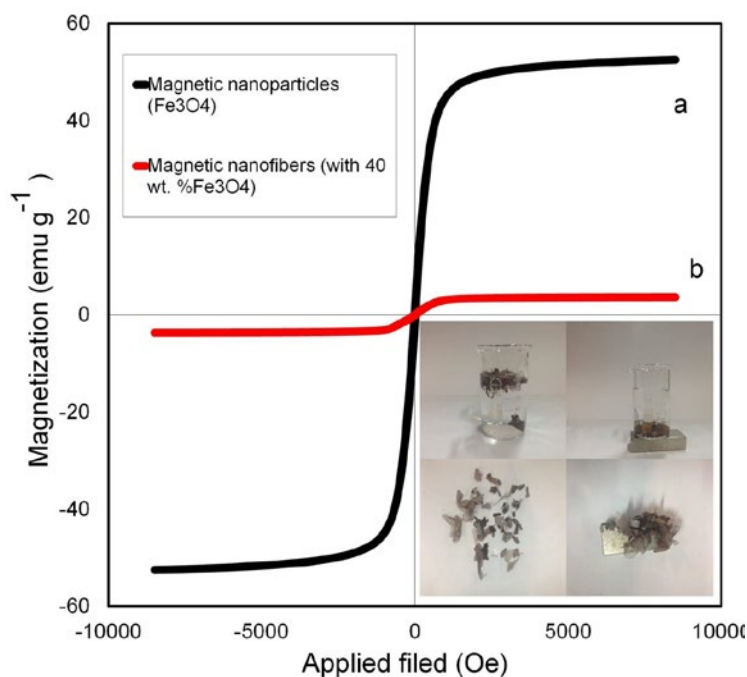


Fig. 9. Hysteresis loops of (a) Fe_3O_4 nanoparticles and (b) PAN-co-AA (40 wt%) / Fe_3O_4 composites nanofibers at room temperature.

in AN segment and C=O in AA segment, respectively [40]. No peak related to C=C stretching vibration absorption around 1600 cm^{-1} was observed, indicating that none of AA and AN monomers remained in copolymers and copolymer was washed properly [41]. In the case of magnetic nanofibers (Fig. S8c), total characteristic peaks of magnetic nanoparticles can be observed in the magnetic nanofibers, thereby demonstrating the successful incorporation of Fe_3O_4 NPs in/on the nanofibers. With the exception of Fe-O- Fe peak (at 586 cm^{-1}), no additional bands appeared in the FT-IR spectra of magnetic nanofibers. These results indicate that the molecular structure of copolymers maintains constant after electrospinning with Fe_3O_4 nanoparticles.

Magnetic properties

The plots of magnetization versus magnetic field (M–H loop) of magnetic nanoparticles and magnetic nanofibers (40 wt. %) at room temperature are illustrated in Fig. 9.

Both samples exhibit a superparamagnetic behavior at room temperature. The magnetization versus field (M–H) shows no coercivity. The hysteresis loop in the single domain is disappearing when the particle size becomes so small that the maximum anisotropy energy approaches to the thermal energy. Under this condition the ferro or ferrimagnetism called “superparamagnetism” as it does not present any hysteresis in M–H graph [42-43].

The saturation magnetization (M_s), remnant magnetization (M_r), coercivity (H_c), and M_r/M_s ratio were estimated at 52.52 emu.g^{-1} , 1.33 emu.g^{-1} , 14.65 Oe , and 0.0253 , for naked magnetic nanoparticles, and 3.64 emu.g^{-1} , 0.0918 emu.g^{-1} , 21.67 Oe , and 0.0252 for magnetic nanofibers, respectively. The decline in M_s value of MNFs is most likely attributed to the MNPs surrounded with polymer [44]. However, as shown in Fig. 9, it is still sufficient for magnetic separation by a conventional magnet.

This magnetic nanofibers, due to desirable properties such as high surface area, high magnetic properties and presence of carbonyl and carboxyl groups on their surface, can be used effectively in adsorption, separation (nanofiltration), solid phase extraction, etc.

CONCLUSION

In conclusion, the ultrafine of PAN-co-AA/ Fe_3O_4 composite nanofibers were fabricated

using electrospinning technique. To achieve bead-free nanofibers with minimum fiber diameter, the effects of electrospinning parameters on fiber morphology were studied. The optimum electrospinning conditions were obtained as follows: polymeric concentration of 12 wt. %, applied voltage of 20 kV, flow rate of 5 mL/h and working distance of 200 mm. Also, flat plate collector was used to produce thinner fiber. When the Fe_3O_4 mass proportion was increased from 0 to 40 wt. %, the fiber diameter dropped from 359 nm to 74 nm. The surface area of MNFs at 0 and 40 wt. % was 9.66 and $12.09\text{ m}^2.\text{g}^{-1}$, respectively. The magnetic properties of nanofibers was about 3.6 emu.g^{-1} , but according to the results, the magnetism is sufficient to carry out separation.

ACKNOWLEDGEMENTS

This work has been financially supported by the support of Quchan University of Advanced Technology (research grant 1019, 15/03/2015).

CONFLICT OF INTEREST

The authors declare that there are no conflicts of interest regarding the publication of this manuscript.

REFERENCES

1. Soofivand F, Salavati-Niasari M, Mohandes F. Novel precursor-assisted synthesis and characterization of zinc oxide nanoparticles/nanofibers. *Materials Letters*. 2013;98:55-8.
2. Ghanbari D, Salavati-Niasari M, Ghasemi-Kooch M. A sonochemical method for synthesis of Fe_3O_4 nanoparticles and thermal stable PVA-based magnetic nanocomposite. *Journal of Industrial and Engineering Chemistry*. 2014;20(6):3970-4.
3. Sangsefidi FS, Esmaili-Zare M, Salavati-Niasari M. Hydrothermal synthesis and characterization of HgS nanostructures assisted by inorganic precursor. *Journal of Industrial and Engineering Chemistry*. 2015;28:197-201.
4. Pebdeni A, Sadri M, Hosseini H. Preparation of Biopolymeric Nanofiber Containing Silica and Antibiotic. *J Nanostruct*. 2016; 6 (1): 96–100.
5. Sabzroo N, Bastami TR, Karimi M, Heidari T, Agarwal S, Gupta VK. Synthesis and characterization of magnetic poly(acrylonitrile- co -acrylic acid) nanofibers for dispersive solid phase extraction and pre-concentration of malachite green from water samples. *Journal of Industrial and Engineering Chemistry*. 2018;60:237-49.
6. Zheng Y, Gong RH, Zeng Y. Multijet motion and deviation in electrospinning. *RSC Advances*. 2015;5(60):48533-40.
7. Xie J, Mao H, Yu D-G, Williams GR, Jin M. Highly stable coated polyvinylpyrrolidone nanofibers prepared using modified coaxial electrospinning. *Fibers and Polymers*. 2014;15(1):78-83.
8. Qin C-C, Duan X-P, Wang L, Zhang L-H, Yu M, Dong R-H, et al. Melt electrospinning of poly(lactic acid) and

- polycaprolactone microfibers by using a hand-operated Wimshurst generator. *Nanoscale*. 2015;7(40):16611-5.
9. Naderizadeh B, Moghimi A, Shahi M. Electrospun Nitrocellulose and Composite Nanofibers. *J Nanostructre*. 2012; 2: 287–293.
 10. Alam A-M, Liu Y, Park M, Park S-J, Kim H-Y. Preparation and characterization of optically transparent and photoluminescent electrospun nanofiber composed of carbon quantum dots and polyacrylonitrile blend with polyacrylic acid. *Polymer*. 2015;59:35-41.
 11. Ismar E, Sarac AS. Synthesis and characterization of poly (acrylonitrile-co-acrylic acid) as precursor of carbon nanofibers. *Polymers for Advanced Technologies*. 2016;27(10):1383-8.
 12. Ndayambaje G, Laatikainen K, Laatikainen M, Beukes E, Fatoba O, van der Walt N, et al. Adsorption of nickel(II) on polyacrylonitrile nanofiber modified with 2-(2'-pyridyl) imidazole. *Chemical Engineering Journal*. 2016;284:1106-16.
 13. Zhu J, Wei S, Rutman D, Haldolaarachchige N, Young DP, Guo Z. Magnetic polyacrylonitrile-Fe@FeO nanocomposite fibers - Electrospinning, stabilization and carbonization. *Polymer*. 2011;52(13):2947-55.
 14. Ye X-Y, Liu Z-M, Wang Z-G, Huang X-J, Xu Z-K. Preparation and characterization of magnetic nanofibrous composite membranes with catalytic activity. *Materials Letters*. 2009;63(21):1810-3.
 15. Zhou S, Liu F, Zhang Q, Chen B-Y, Lin C-J, Chang C-T. Preparation of Polyacrylonitrile/Ferrous Chloride Composite Nanofibers by Electrospinning for Efficient Reduction of Cr(VI). *Journal of Nanoscience and Nanotechnology*. 2015;15(8):5823-32.
 16. Wang Z-G, Ke B-B, Xu Z-K. Covalent immobilization of redox enzyme on electrospun nonwoven poly(acrylonitrile-co-acrylic acid) nanofiber mesh filled with carbon nanotubes: A comprehensive study. *Biotechnology and Bioengineering*. 2006;97(4):708-20.
 17. Bayat M, Yang H, Ko F. Electromagnetic properties of electrospun Fe₃O₄/carbon composite nanofibers. *Polymer*. 2011;52(7):1645-53.
 18. Qiao H, Chen F, Xia X, Wei F, Huang L. Characterization of Polyaniline/Fe₃O₄-Polyacrylonitrile Composite Nanofibers. *J Fiber Bioeng Informatics*. 2010; 2 (4): 253–258.
 19. Oak S, Kobayashi T, Wang Y, Fukaya T, Fujii N. pH Effect on Molecular Size Exclusion of Polyacrylonitrile Ultrafiltration Membranes Having Carboxylic Acid Groups. *J Memb Sci*. 1997; 123: 185–195.
 20. Zhang D, Karki AB, Rutman D, Young DP, Wang A, Cocke D, et al. Electrospun polyacrylonitrile nanocomposite fibers reinforced with Fe₃O₄ nanoparticles: Fabrication and property analysis. *Polymer*. 2009;50(17):4189-98.
 21. Han J, Wu Q, Xia Y, Wagner MB, Xu C. Cell alignment induced by anisotropic electrospun fibrous scaffolds alone has limited effect on cardiomyocyte maturation. *Stem Cell Research*. 2016;16(3):740-50.
 22. Che A-F, Liu Z-M, Huang X-J, Wang Z-G, Xu Z-K. Chitosan-Modified Poly(acrylonitrile-co-acrylic acid) Nanofibrous Membranes for the Immobilization of Concanavalin A. *Biomacromolecules*. 2008;9(12):3397-403.
 23. Qi X-Y, Yan D, Jiang Z, Cao Y-K, Yu Z-Z, Yavari F, et al. Enhanced Electrical Conductivity in Polystyrene Nanocomposites at Ultra-Low Graphene Content. *ACS Applied Materials & Interfaces*. 2011;3(8):3130-3.
 24. Shakouri-Arani M, Salavati-Niasari M. Synthesis and characterization of wurtzite ZnS nanoplates through simple solvothermal method with a novel approach. *Journal of Industrial and Engineering Chemistry*. 2014;20(5):3179-85.
 25. Lu Y, Li Y, Zhang S, Xu G, Fu K, Lee H, et al. Parameter study and characterization for polyacrylonitrile nanofibers fabricated via centrifugal spinning process. *European Polymer Journal*. 2013;49(12):3834-45.
 26. Ribeiro C, Sencadas V, Costa CM, Gómez Ribelles JL, Lanceros-Méndez S. Tailoring the morphology and crystallinity of poly(L-lactide acid) electrospun membranes. *Science and Technology of Advanced Materials*. 2011;12(1):015001.
 27. Liu J, Huang J, Wujcik EK, Qiu B, Rutman D, Zhang X, et al. Hydrophobic Electrospun Polyimide Nanofibers for Self-cleaning Materials. *Macromolecular Materials and Engineering*. 2015;300(3):358-68.
 28. Mahmoodi V, Ahmadpour A, Rohani Bastami T, Hamed Mousavian MT. Facile Synthesis of BiOI Nanoparticles at Room Temperature and Evaluation of their Photoactivity Under Sunlight Irradiation. *Photochemistry and Photobiology*. 2017;94(1):4-16.
 29. Ramazani, S, Karimi M. Electrospinning of PCL Solution Containing Graphene Oxide: Effects of Graphene Oxide Content and Oxidation level. *Polym Polym Compos*. 2008; 16 (2): 101–13.
 30. Schima A. Electrospinning of Aligned Fibers with Adjustable Orientation using Auxiliary Electrodes. *Sci Technol Adv Mater*. 2012; 13 (3): 35008- 35011.
 31. Bizarria MTM, d'Ávila MA, Mei LHI. Non-woven nanofiber chitosan/peo membranes obtained by electrospinning. *Brazilian Journal of Chemical Engineering*. 2014;31(1):57-68.
 32. Wang S-H, Wan Y, Sun B, Liu L-Z, Xu W. Mechanical and electrical properties of electrospun PVDF/MWCNT ultrafine fibers using rotating collector. *Nanoscale Research Letters*. 2014;9(1).
 33. Baji A, Mai Y-W, Wong S-C, Abtahi M, Chen P. Electrospinning of polymer nanofibers: Effects on oriented morphology, structures and tensile properties. *Composites Science and Technology*. 2010;70(5):703-18.
 34. Wang Q, Yu D-G, Zhang L-L, Liu X-K, Deng Y-C, Zhao M. Electrospun hypromellose-based hydrophilic composites for rapid dissolution of poorly water-soluble drug. *Carbohydrate Polymers*. 2017;174:617-25.
 35. Eichhorn SJ, Sampson WW. Relationships between specific surface area and pore size in electrospun polymer fibre networks. *Journal of The Royal Society Interface*. 2010;7(45):641-9.
 36. Rohani Bastami T, Ahmadpour A, Ahmadi Hekmatikar F. Synthesis of Fe₃O₄/Bi₂WO₆ nanohybrid for the photocatalytic degradation of pharmaceutical ibuprofen under solar light. *Journal of Industrial and Engineering Chemistry*. 2017;51:244-54.
 37. Atar N, Eren T, Yola ML, Karimi-Maleh H, Demirdögen B. Magnetic iron oxide and iron oxide@gold nanoparticle anchored nitrogen and sulfur-functionalized reduced graphene oxide electrocatalyst for methanol oxidation. *RSC Advances*. 2015;5(33):26402-9.
 38. Bastami TR, Entezari MH. Activated carbon from carrot dross combined with magnetite nanoparticles for the efficient removal of p-nitrophenol from aqueous solution. *Chemical Engineering Journal*. 2012;210:510-9.
 39. Bastami TR, Entezari MH, Hu QH, Hartono SB, Qiao SZ. Role

- of polymeric surfactants on the growth of manganese ferrite nanoparticles. *Chemical Engineering Journal*. 2012;210:157-65.
40. Xu Y, Zhuang L, Lin H, Shen H, Li JW. Preparation and characterization of polyacrylic acid coated magnetite nanoparticles functionalized with amino acids. *Thin Solid Films*. 2013;544:368-73.
41. Lin Y-J, Hsu F-C, Chou C-W, Wu T-H, Lin H-R. Poly(acrylic acid)-chitosan-silica hydrogels carrying platelet gels for bone defect repair. *J Mater Chem B*. 2014;2(47):8329-37.
42. Bastami TR, Entezari MH. Synthesis of manganese oxide nanocrystal by ultrasonic bath: Effect of external magnetic field. *Ultrasonics Sonochemistry*. 2012;19(4):830-40.
43. Rohani Bastami T, Entezari MH. A novel approach for the synthesis of superparamagnetic Mn₃O₄ nanocrystals by ultrasonic bath. *Ultrasonics Sonochemistry*. 2012;19(3):560-9.
44. Liu Q, Zhong L-B, Zhao Q-B, Frear C, Zheng Y-M. Synthesis of Fe₃O₄/Polyacrylonitrile Composite Electrospun Nanofiber Mat for Effective Adsorption of Tetracycline. *ACS Applied Materials & Interfaces*. 2015;7(27):14573-83.
45. Che A-F, Huang X-J, Wang Z-G, Xu Z-K. Preparation and Surface Modification of Poly(acrylonitrile-co-acrylic acid) Electrospun Nanofibrous Membranes. *Australian Journal of Chemistry*. 2008;61(6):446.
46. Saallah S, Naim MN, Lenggoro IW, Mokhtar MN, Abu Bakar NF, Gen M. Immobilisation of cyclodextrin glucanotransferase into polyvinyl alcohol (PVA) nanofibres via electrospinning. *Biotechnology Reports*. 2016;10:44-8.
47. Wu H, Zhang R, Liu X, Lin D, Pan W. Electrospinning of Fe, Co, and Ni Nanofibers: Synthesis, Assembly, and Magnetic Properties. *Chemistry of Materials*. 2007;19(14):3506-11.
48. Wang J, Pan K, Giannelis EP, Cao B. Polyacrylonitrile/polyaniline core/shell nanofiber mat for removal of hexavalent chromium from aqueous solution: mechanism and applications. *RSC Advances*. 2013;3(23):8978.
49. Ma G, Yang D, Nie J. Preparation of porous ultrafine polyacrylonitrile (PAN) fibers by electrospinning. *Polymers for Advanced Technologies*. 2009;20(2):147-50.
50. Almasian A, Olya ME, Mahmoodi NM. Synthesis of polyacrylonitrile/polyamidoamine composite nanofibers using electrospinning technique and their dye removal capacity. *Journal of the Taiwan Institute of Chemical Engineers*. 2015;49:119-28.
51. Wang Y, Yang Q, Shan G, Wang C, Du J, Wang S, et al. Preparation of silver nanoparticles dispersed in polyacrylonitrile nanofiber film spun by electrospinning. *Materials Letters*. 2005;59(24-25):3046-9.